Band Alignment of Sb_2O_3 and Sb_2Se_3

Huw Shiel†, Theodore D. C. Hobson†, Oliver S. Hutter‡, Laurie J. Phillips†, Matthew J. Smiles†, Leanne A. H. Jones†, Thomas J. Featherstone†, Jack E. N. Swallow§, Pardeep K. Thakur∓, Tien-Lin Lee∓, Jonathan D. Major†, Ken Durose†, and Tim D. Veal†

†*Stephenson Institute for Renewable Energy and Department of Physics, University of Liverpool, Liverpool L69 7ZF, United Kingdom.*

‡*Department of Mathematics, Physics and Electrical Engineering, Northumbria University, Newcastle upon Tyne NE1 8ST, United Kingdom.*

§*Department of Materials, University of Oxford, Parks Road, Oxford OX1 3PH, UK and*

∓ *Diamond Light Source, Harwell Science and Innovation Campus, Didcot, UK, OX11 0DE*

Antimony selenide (Sb_2Se_3) possesses great potential in the field of photovoltaics (PV) due to its suitable properties for use as a solar absorber and good prospects for scalability. Previous studies have reported the growth of a native antimony oxide (Sb_2O_3) layer at the surface of Sb_2Se_3 thin films during deposition and exposure to air, which can affect the contacting between Sb_2Se_3 and subsequent layers. In this study, photoemission techniques were utilised on both Sb_2Se_3 bulk crystals and thin films to investigate the band alignment between Sb_2Se_3 and the Sb_2O_3 layer. By subtracting the valence band spectrum of an *in situ* cleaved Sb_2Se_3 bulk crystal from that of the atmospherically contaminated bulk crystal, a valence band offset (VBO) of -1.72 eV is measured between Sb_2Se_3 and Sb_2O_3. This result is supported by a -1.90 eV VBO measured between Sb_2O_3 and Sb_2Se_3 thin films via the Kraut method. Both results indicate a straddling alignment which would oppose carrier extraction through the back contact of superstrate PV devices. This work yields greater insight into the band alignment of Sb_2O_3 at the surface of Sb_2Se_3 films, which is crucial for improving the performance of these PV devices.

I. INTRODUCTION

Sb_2Se_3 has attracted much attention in recent years for its potential as an absorber layer in photovoltaics (PV) and photocatalysis. It has experienced a rapid rise in PV performance, from ∼2% to nearly 10% in only a few years [1, 2]. The material has a very high absorption coefficient and a band gap of 1.18 eV, making it a good candidate for use in PV [3, 4]. Furthermore, Sb and Se are Earth-abundant and low-cost [5], and Sb_2Se_3 can be fabricated via a wide variety of scalable methods [6–10]. Sb_2Se_3 also attracts great interest due to its unusual 1D nanoribbon structure and $5s^2$ lone pair of electrons [3, 11, 12]. This structure means that strong, covalently bonded 1D nanoribbons are bound by weaker van der Waals interactions in two dimensions.

Several studies have evidenced the formation of an Sb_2O_3 contaminant layer on the surface of Sb_2Se_3 thin films and crystals alike [12–14]. This has attracted interest from a PV perspective due to the implications of an intermediate layer between the Sb_2Se_3 and a back contact layer for charge transport/extraction in superstrate devices [13, 15](and could also have implications for heterojunction formation in substrate devices). This relies heavily on both the conductivity of the Sb_2O_3 interlayer and the band alignments between Sb_2Se_3, Sb_2O_3 and the metal contact. However, a full understanding of this oxide is difficult due its contaminant nature. Band alignment estimates from natural band positions with respect to the vacuum level are avoided here as they do not account for any charge transfer at the real interface and natural alignment measurements using photoemission are difficult for very wide band gap materials. Furthermore there is significant variation in the reported ionisation potential of Sb_2O_3 in the literature [16, 17]. Previously, attempts have been made to reproduce the effects of the native oxide through deposition of an ultra-thin Sb_2O_3 film at the back surface [15], however a clearer analysis is possible using bulk crystals.

The aforementioned crystal structure of Sb_2Se_3 means that, in two spatial directions, highly oriented bulk crystals can be easily cleaved or exfoliated to expose a pristine surface. In this study, bulk crystals with natively grown oxide were cleaved in-situ to allow photoemission measurements of the valence band both with and without this surface contamination. A valence band subtraction method was used to measure the VBO between these two layers without having to destructively remove the contamination or attempt to reproduce it with another method. This subtraction method was used previously by Fleck *et al.* but no quantitative analysis was carried out [15]. Additionally, thermally evaporated thin films are used to measure the band alignment between Sb_2O_3 and close space sublimation (CSS) grown Sb_2Se_3 via the Kraut method (a common technique used to determine valence band offsets between materials) for comparison [18].

II. METHODS

The Sb_2Se_3 bulk crystals were fabricated via the Bridgman melt-growth technique using a single-zone

vertical furnace. A sealed ampoule containing manually ground Sb_2Se_3 granules (5N purity, Alfa Aesar) was placed with the bottom tip in line with the peak of the temperature profile in the furnace and heated to 620°C to melt the source material. It was then held for around 6 hours to allow full melting and homogenisation of the powder. The ampoule was then lowered through the natural temperature gradient of the furnace at 0.6°C/mm towards the lower, open end of the furnace (at room temperature), at a rate of 1.15 mm/hour for 7 days. The ampoule was rotated slowly throughout to ensure homogeneous heating. A more detailed description of the process and characterisation of the crystals is provided elsewhere [12, 19–22].

Three thin film samples were used in this work to carry out the Kraut method. A thick film of each material (Sb_2Se_3 & Sb_2O_3) was required to measure core level and VBM binding energy as well as an 'interfacial' sample - a thin layer of Sb_2O_3 on Sb_2Se_3 to measure core level binding energies. A ∼2 μm thick Sb_2Se_3 film was deposited via CSS onto solution processed TiO_2 films on FTO-coated glass substrates (matching the usual solar cell structure [6, 19]). A two stage process was used - 2 minutes with a source temperature of 390°C, substrate heating at 360°C and a pressure of ∼0.05 Torr followed by 15 minutes with a source temperature of 470°C at a pressure of 10 Torr. A ∼75 nm thick film of Sb_2O_3 was deposited via thermal evaporation onto a fluorine doped SnO_2 (FTO) coated glass substrate. A thin Sb_2O_3 film was deposited onto Sb_2Se_3 for the interface measurement. Sb_2O_3 thickness was limited to 22 nm, as determined using atomic force microscopy and the Sb_2Se_3 layer was identical to the thick Sb_2Se_3 sample. More detailed descriptions of the process and characterisation of the films has been carried out elsewhere [6, 23, 24].

Hard x-ray photoemission spectroscopy was carried out at the I09 beamline at the Diamond Light Source facility. An x-ray energy of 5.921 keV was selected using a double-crystal Si(111) monochromator followed by a Si(004) channel-cut crystal. The energy resolution was 250 meV, determined by fitting a Gaussian-broadened Fermi-Dirac distribution to the Fermi edge of a gold reference sample. A Scienta Omicron EW4000 high-energy analyser was used to acquire the data, with an acceptance angle of ±28°. All spectra were calibrated using the Fermi level of a Au reference sample. Following the initial, as-received measurement, the crystals were cleaved in-situ to expose a pristine (010) surface (in the Pbnm space group setting [25]), as demonstrated by Hobson *et al.* and Don *et al.* in previous works by our group [12, 19]. All peak positions from curve fitting are reported with an error of ±0.05 eV. HAXPES core level spectra were curve fitted using CASAXPS software with Voigt lineshapes after subtracting a Shirley background [26].

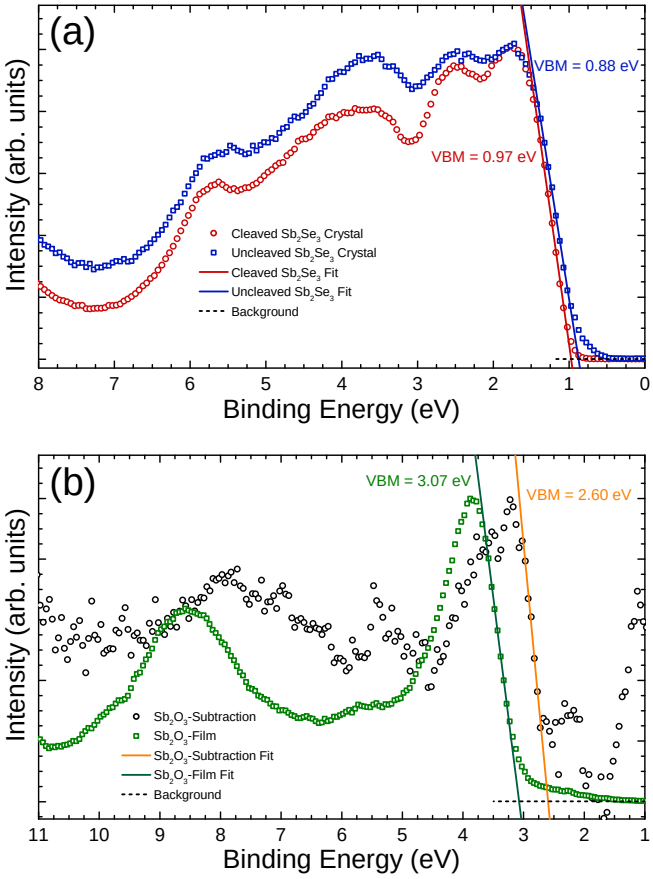

FIG. 1: (a) Valence band spectra of (red) cleaved Sb_2Se_3 crystal and (blue) uncleaved Sb_2Se_3 crystal and (b) valence band spectra of (green) Sb_2O_3 thin film and (black) valence band subtracted Sb_2O_3. All spectra are shown with linear fits and measured VBM energies. Data for part (a) is reproduced with permission from J. Mater. Chem. C **8**, 12615 (2020). CC-BY 4.0.

III. RESULTS

The valence band spectra of a highly-oriented bulk crystal material can provide a wealth of information about its electronic properties. Figure 1a shows the valence band spectra of an Sb_2Se_3 bulk crystal both prior to and after *in situ* cleaving to remove any surface contamination. Straight line fits are used to determine the energy position of the leading edge - this energy is representative of the separation between the valence band maximum (VBM) and the Fermi level and henceforth any reference to VBM is a reference to the energy separation between the valence band and Fermi level. The results of this fit are a valence band to Fermi level separation of 0.88 eV and 0.97 eV for the uncleaved and cleaved Sb_2Se_3 crystals respectively. This difference has significant implications for PV technology, as has been discussed in other works [15].

Figure 1a shows the valence band spectra of the

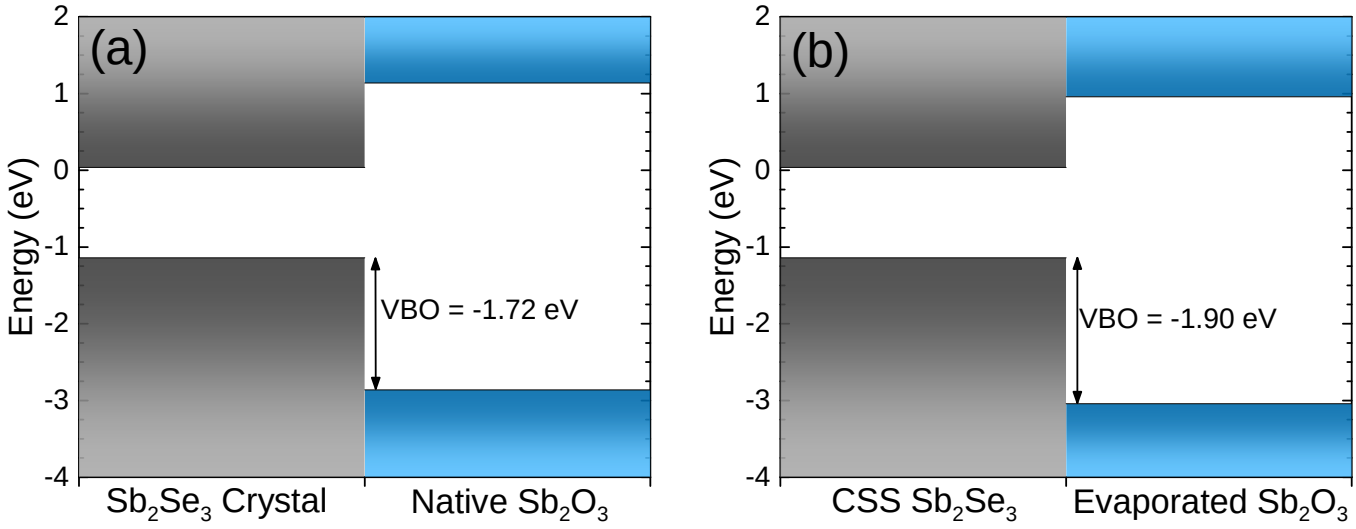

FIG. 2: Band alignment between (a) Sb_2Se_3 bulk crystal and its native Sb_2O_3 determined by valence band subtraction and (b) close space sublimation-deposited Sb_2Se_3 and a thermally evaporated Sb_2O_3 thin film determined using the Kraut method. Conduction band energies have been determined by adding the known band gap values for Sb_2Se_3 and Sb_2O_3 of 1.18 eV and 4 eV.

Sb_2Se_3 bulk crystal before and after *in situ* cleaving. The spectra show some difference in intensity at binding energies above 3 eV and this difference is particularly pronounced between 3 and 4 eV. As previously reported by Don *et al.* [12], this intensity difference is attributed to a surface layer of Sb_2O_3 that is known to grow on the surface of Sb_2Se_3 upon exposure to air. The two spectra have been normalised to be matching in intensity at ∼1.7 eV [27]. This point was chosen for the normalisation for two reasons - firstly the shapes of the valence bands are very similar up to ∼2 eV, with the shape of the spectrum from the uncleaved sample beginning to differ towards higher binding energy. By normalising to this point there is no negative intensity in the difference spectrum [27], with the contribution from the Sb_2O_3 beginning to show from ∼2 eV. This point also corresponds to the binding energy at which the Sb 5s orbital has a significant contribution in the Sb_2Se_3 density of states [12]. It therefore corresponds to a peak in the valence band density of states (rather than background intensity or a peak shoulder/edge), making it more reliable. Secondly, at this point no contribution from Sb_2O_3 would be expected (due to its wide band gap and n-type conductivity), meaning that the intensity at this point originates solely from Sb_2Se_3 in both spectra. No energy shift was necessary to align the two samples, which lent weight to the assumption that the valence band edge position was representative of the Sb_2Se_3's VBM-E_F separation in both the oxidised and pristine states. By subtracting the cleaved spectrum from the uncleaved, the remaining intensity, called the difference spectrum, should originate from this Sb_2O_3 layer [27]. This is shown by the black circular data points in Figure 1b and will henceforth be referred to as 'Sb_2O_3-sub'.

To ascertain whether this method was successful, the Sb_2O_3-sub difference spectrum was compared to the valence band spectrum of a thin film of Sb_2O_3 (henceforth referred to as 'Sb_2O_3-film'). This is a thermally evaporated thin film deposited onto Sb_2Se_3 but with a thickness of 75 nm. This data is represented by the green square data points on Figure 1b and shows good agreement with the Sb_2O_3-sub data. Both exhibit a peak in intensity at the edge of the valence band, with another broader feature at 5-6 eV below the valence band edge. However, the two spectra do not line up in energy, with the Sb_2O_3-film valence band lying roughly 0.5 eV to higher binding energy than Sb_2O_3-sub. There is also a peak in the Sb_2O_3-sub spectrum at 1 eV, corresponding exactly with the edge of the Sb_2Se_3 data. This spike is attributed to a difference in mid-gap states between the air exposed crystal and the *in situ* cleaved crystal [28, 29].

Again using linear fits, the VBM energies were determined to be 3.07 eV and 2.60 eV respectively for the Sb_2O_3-film and Sb_2O_3-sub. This highlights a difference between the deposited film and the native oxide, although whether this is due to a difference in thickness or has a different origin is unclear (as discussed below). Using the valence band edge of the Sb_2O_3-sub, it is possible to determine the band alignment between the valence band of Sb_2Se_3 and Sb_2O_3 contamination.

The band gap of Sb_2Se_3 is well known to be 1.18 eV [4] while there is a range of reported band gap values for Sb_2O_3, from ∼3.6 eV to ∼4 eV [30–32]. For this

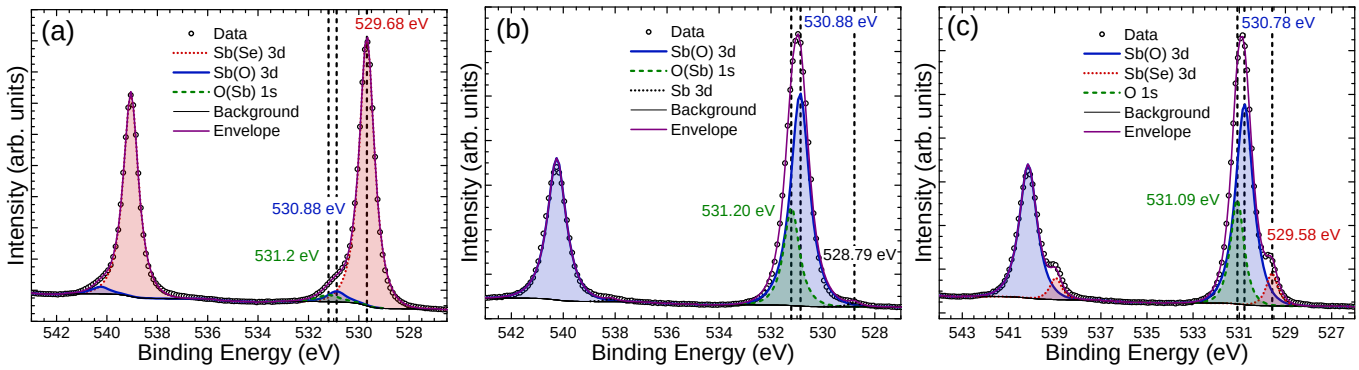

FIG. 3: Core level spectra of the Sb 3d and O 1s region for (a) Sb_2Se_3 thin film, (b) Sb_2O_3 thin film and (c) Sb_2O_3/Sb_2Se_3 interfacial sample.

study we have used a DFT calculated band gap of approximately 4 eV [33]. This was calculated using the HSE06 functional which is known to achieve accurate band gap values and is in line with many values reported in the literature [30–32]. This is towards the upper limit of the range reported in the literature but, as will be shown later, any smaller values within the reported range would have no bearing on the conclusions of this work - the nature of the conduction band offset is the same for all reasonable values of the Sb_2O_3 band gap. Using the valence band subtraction method, the VBO between Sb_2Se_3 and Sb_2O_3 can be measured as the difference in the two valence band edge energies of the uncleaved crystal and the native oxide from the Sb_2O_3-sub spectrum. Figure 2a shows the resulting experimentally determined band alignment between Sb_2Se_3 and its native oxide. The VBO of -1.72 eV shown in Figure 2a implies a straddling alignment (where both the CBM and VBM of one material lie within the band gap of the other), as would be expected with two materials of such different band gaps. An uncertainty of 0.14 eV was determined for the linear fitting procedure, which is not sufficient to change the straddling nature of the alignment.

In order to verify the nature of the alignment between Sb_2Se_3 and Sb_2O_3, the VBO between thin films of Sb_2Se_3 and Sb_2O_3 was measured via the Kraut method. This method is widely used to directly measure the offset between the valence bands of one material deposited on another using equation 1. E_{CL}^X denotes the core level binding energy of material X, E_V^X is the binding energy of the VBM of material X and ΔE_{CL} represents the binding energy separation of two core levels from the different materials in the interfacial sample.

$$\Delta E_V = ({E_{CL}}^B\text{-}{E_V}^B) - ({E_{CL}}^A\text{-}{E_V}^A) + \Delta E_{CL} \qquad (1)$$

By taking advantage of the fact that the band energy shift that occurs upon interface formation is consistent for the valence band, conduction band and, importantly, core-levels, this method allows the true offset to be determined as long as the top layer is thin enough to enable the photoelectrons from the substrate layer to pass through the top layer [18]. The use of HAXPES allows for depths of ∼30 nm to be probed, much greater than XPS (∼10 nm) or UPS (∼2 nm) [23]. For this measurement, an Sb_2O_3 layer was deposited to a thickness of 22 nm onto a 1.5 μm thick layer of Sb_2Se_3. Separate, thicker layers of Sb_2Se_3 (2 μm) and Sb_2O_3 (75 nm) were also used for the measurement. In equation 1, the energy separation between a core levels and the valence band edge, (E_{CL}-E_V), is measured for a thick film of each material and then the energy separation between core levels from each material, ΔE_{CL}, is measured for the thin interfacial sample.

Figure 3 shows the HAXPES core level spectra of the Sb 3d and O 1s region for the Sb_2Se_3, Sb_2O_3 and Sb_2O_3/Sb_2Se_3 interface thin films. The spectrum from the Sb_2Se_3 film (Figure 3a) is, as expected, dominated by Sb bonded to Se, with a very small contribution from Sb bonded to O. This is a result of oxidation of the surface when the sample was briefly exposed to air. The signal is so small that it does not indicate a complete layer of Sb_2O_3, such as the one removed by *in situ* cleaving [12]. The spectrum from the Sb_2O_3 film (Figure 3b) is dominated by Sb bonded to O, as well as the overlapping O 1s peak. This sample also shows some trace contamination from metallic Sb at 528.79 eV, likely a by-product of the deposition process or some slight oxygen deficiency in the source material. The interfacial sample (Figure 3c) shows signals from both Sb_2Se_3 and Sb_2O_3 with the oxide signal dominating as expected for the uppermost layer. Other core levels used for the Kraut method calculations as well as valence band spectra for the thin films are included in Supplementary Figures S1–S4.

Figure 2b shows the VBO as measured by the Kraut method. The measured VBO was -1.90 eV, taken as an

average of the different valence band offsets calculated using different combinations of core level peaks (see Table S2). The error on the measurement was taken as the standard deviation of the different calculated values and was determined to be 0.13 eV. The offset of -1.90±0.13 eV is consistent with that determined by the subtraction method and would also signify a straddling alignment. For detailed breakdown of measured peak positions and valence band offsets see Supplementary Tables S1 & S2.

IV. DISCUSSION

While the two VBO values determined for the native oxide on Sb_2Se_3 crystal and the evaporated Sb_2O_3 on Sb_2Se_3 film are consistent with each other, there are several possible reasons for any small differences. These include how the native oxide forms on the surface, which occurs under very different conditions from a thermally evaporated film, and has been shown to be accompanied by elemental selenium at the surface (equation 2) [15]. Additionally, the crystal surface studied is made up of only one crystal orientation, whereas the polycrystalline film's surface includes multiple different orientations [6, 19, 34]. Ultimately, however, the two results can be considered consistent with each other taking into account the uncertainty on the values, which was taken as the standard deviation in the calculated values (0.13 eV) for the Kraut method results and as 0.14 eV for the subtraction method (determined from the uncertainty in the linear extrapolation of the valence band onsets).

$$2\,Sb_2Se_3 + 3\,O_2 \longrightarrow 2\,Sb_2O_3 + 3\,Se_2 \qquad (2)$$

These results have implications for Sb_2Se_3's use as a PV material due to the great difficulty in avoiding Sb_2O_3 formation at the back surface, as reported by Fleck *et al.* [15]. The presence of Sb_2O_3 between the Sb_2Se_3 layer and the back contact had a significant effect on the degree of 'rollover' (a feature in J-V curves indicative of a back contact potential barrier) in Sb_2Se_3 solar cells and the formation of Ohmic contacts. Attempts to remove this Sb_2O_3 contamination have also been shown to have mixed effects on the performance of the PV devices [13, 14]. Fleck *et al.* also attempted to replicate the effects of Sb_2O_3 contamination by depositing ultra-thin films of Sb_2O_3 onto the back contact via thermal evaporation. They reported that a thin layer of Sb_2O_3 could suppress recombination at the interface between Sb_2Se_3 and Au provided the holes could tunnel through the Sb_2O_3 layer. Thicker layers of Sb_2O_3, even up to 5 nm, were found to be detrimental to device performance. This is supported by the conclusions of this work, which shows that any significant thickness of Sb_2O_3 would provide a significant barrier to hole transport through the back contact due to the magnitude of the negative VBO.

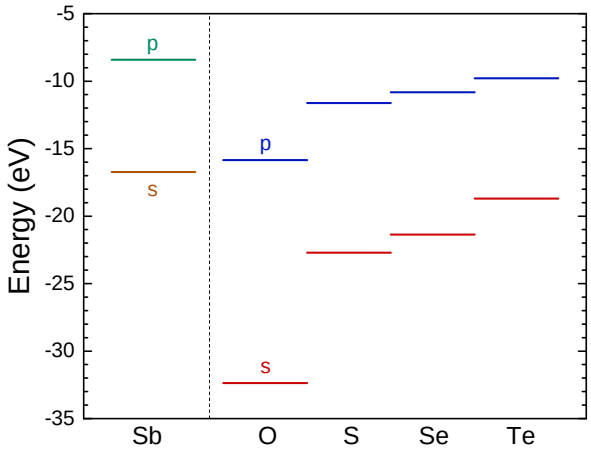

FIG. 4: Orbital energies of Sb and the chalcogenide series. Data taken from Ref. 35.

The significant offset between the two valence bands can be explained by looking in greater detail at the valence orbital density of states for the two materials. Antimony chalcogenides are known to exhibit strong cation s - anion p orbital mixing, leading to the existence of a stereochemically-active lone pair of electrons at the valence band edge [12, 36]. The mixing of the cation s states with the anion p states results in the formation of bonding and anti-bonding states. The anti-bonding states in turn hybridise with the cation p orbitals to form bonding and anti-bonding states that make up the edges of the valence and conduction bands respectively. The configuration energies of the anion p-orbitals therefore play a significant role in determining the position of the valence band maximum on an absolute energy scale and this has been shown to result in a lower ionisation potential in materials containing these lone pairs compared to those without. Both Sb_2Se_3 and Sb_2O_3 are predicted to undergo this lone pair formation (experimentally evidenced for Sb_2Se_3 by Don *et al.* [12]) but, as shown in Figure 4, there is a significant 'jump' in the orbital energies when going from sulphur to oxygen in the chalcogenide series, with the selenium orbital energies being similar to those of sulphur [35]. The valence band of Sb_2O_3 would therefore be expected to sit significantly lower (or have a higher ionisation potential) than that of Sb_2Se_3, as seen experimentally in this work.

V. CONCLUSIONS

The band alignment between Sb_2O_3 and Sb_2Se_3 was measured via two methods. The first method subtracted the valence band spectra of a native oxide-contaminated

from an *in situ* cleaved bulk Sb_2Se_3 crystal, while the second utilised the Kraut method for a thermally evaporated Sb_2O_3 film on a polycrystalline Sb_2Se_3 grown by close space sublimation. A VBO of -1.72±0.14 eV was measured via the valence band subtraction method between an Sb_2Se_3 crystal and the contaminant native Sb_2O_3 layer, leading to a straddling alignment. This is supported by a similar result obtained by the Kraut method, which yielded a VBO of -1.90±0.13 eV between a Sb_2O_3 thin film grown on Sb_2Se_3. The small difference in the two valence band offsets, however, may be due to differences in the electronic properties of the thermally evaporated film and the native oxide contamination as well as the different Sb_2Se_3 surfaces. The magnitude of the VBO can be explained by examining the orbital energies of the chalcogenide series. Due to the presence of a stereochemically active lone pair at the valence band edge, the chalcogenide p orbital plays a major role in determining the band edge position of the series. As such, there is a significant drop in p orbital energy and increase in ionisation potential moving up the chalcogenide series from selenium and sulphur to oxygen. These results further the understanding of the crucial interface at oxidised Sb_2Se_3 surfaces, and this novel band alignment information can be used to further Sb_2Se_3 device performance.

VI. ACKNOWLEDGEMENTS

The Engineering and Physical Sciences Research Council (EPSRC) is acknowledged for funding of H.S. (Grant No. EP/N509693/1), T.D.C.H. and K.D. (Grant No. EP/T006188/1), O.S.H. (Grant No. EP/M024768/1), L.A.H.J. (Grant No. EP/R513271/1), J.E.N.S., T.J.F., and M.J.S. (Grant No. EP/L01551X/1), J.D.M. (Grant No. EP/N014057/1), and V.R.D. and T.D.V. (Grant No. EP/N015800/1). Paul Warren of NSG Group is thanked for discussions, funding of H.S. and for supplying coated glass substrates. Diamond Light Source is acknowledged for I09 beam time under proposal SI23160-1.

VII. DATA AVAILABILITY STATEMENT

The data that supports the findings of this study are available within the article and its supplementary material.

[1] X. Liu, J. Chen, M. Luo, M. Leng, Z. Xia, Y. Zhou, S. Qin, D.-J. Xue, L. Lv, H. Huang, D. Niu, and J. Tang, Thermal evaporation and characterisation of Sb_2Se_3 thin films for substrate Sb_2Se_3/CdS solar cells, ACS Applied Materials & Interfaces **6**, 10687 (2014).

[2] Z. Li, X. Liang, G. Li, H. Liu, H. Zhang, J. Guo, J. Chen, K. Shen, X. San, W. Yu, R. E. I. Schropp, and Y. Mai, 9.2%-efficient core-shell structured antimony selenide nanorod array solar cells, Nature Communications **10**, 1 (2019).

[3] K. Zeng, D.-J. Xue, and J. Tang, Antimony selenide thin-film solar cells, Semiconductor Science and Technology **31**, 063001 (2016).

[4] M. Birkett, W. M. Linhart, J. Stoner, L. J. Phillips, K. Durose, J. Alaria, J. D. Major, R. Kudrawiec, and T. D. Veal, Band gap temperature-dependence of close-space sublimation grown Sb_2Se_3 by photo-reflectance, APL Materials **6**, 084901 (2018).

[5] U. S. Geological Survey, Mineral commodity summaries 2020 (2020).

[6] L. J. Phillips, C. N. Savory, O. S. Hutter, P. J. Yates, H. Shiel, S. Mariotti, L. Bowen, M. Birkett, K. Durose, D. O. Scanlon, and J. D. Major, Current enhancement via a TiO_2 window layer for CSS Sb_2Se_3 solar cells: performance limits and high V_{oc}, IEEE Journal of Photovoltaics **9**, 544 (2019).

[7] C. Chen, L. Wang, L. Gao, D. Nam, D. Li, K. Li, Y. Zhao, C. Ge, H. Cheong, H. Liu, H. Song, and J. Tang, 6.5% certified efficiency Sb_2Se_3 solar cells using PbS colloidal quantum dot film as hole-transporting layer, ACS Energy Letters **2**, 2125 (2017).

[8] X. Wen, C. Chen, S. Lu, K. Li, R. Kondrotas, Y. Zhao, W. Chen, L. Gao, C. Wang, J. Zhang, G. Niu, and J. Tang, Vapor transport deposition of antimony selenide thin film solar cells with 7.6% efficiency, Nature Communications **9**, 2179 (2018).

[9] R. Tang, Z.-H. Zheng, Z.-H. Su, X.-J. Li, Y.-D. Wei, X.-H. Zhang, Y.-Q. Fu, J.-T. Luo, P. Fan, and G.-X. Liang, Highly efficient and stable planar heterojunction solar cell based on sputtered and post-selenized Sb_2Se_3 thin film, Nano Energy **64**, 103929 (2019).

[10] X. Wang, R. Tang, Y. Yin, H. Ju, S. Li, C. Zhu, and T. Chen, Interfacial engineering for high efficiency solution processed Sb_2Se_3 solar cells, Solar Energy Materials and Solar Cells **189**, 5 (2019).

[11] F. Pattini, S. Rampino, F. Mezzadri, D. Calestani, G. Spaggiari, M. Sidoli, D. Delmonte, A. Sala, E. Gilioli, and M. Mazzer, Role of the substrates in the ribbon orientation of Sb_2Se_3 films grown by low-temperature pulsed electron deposition, Solar Energy Materials and Solar Cells **218**, 110724 (2020).

[12] C. H. Don, H. Shiel, T. D. C. Hobson, C. N. Savory, J. E. N. Swallow, M. J. Smiles, L. A. H. Jones, T. J. Featherstone, P. K. Thakur, T.-L. Lee, K. Durose, J. D. Major, V. R. Dhanak, D. O. Scanlon, and T. D. Veal, Sb $5s^2$ lone pairs and band alignment of Sb_2Se_3: a photoemission and density functional theory study, J. Mater. Chem. C **8**, 12615 (2020).

[13] H. Shiel, O. S. Hutter, L. J. Phillips, M. A. Turkestani, V. R. Dhanak, T. D. Veal, K. Durose, and J. D. Major, Chemical etching of Sb_2Se_3 solar cells: surface chemistry and back contact behaviour, Journal of Physics: Energy **1**, 045001 (2019).

[14] C. Chen, Y. Zhao, S. Lu, K. Li, Y. Li, B. Yang, W. Chen, L. Wang, D. Li, H. Deng, F. Yi, and J. Tang, Accelerated optimization of TiO_2/Sb_2Se_3 thin film solar cells by high-throughput combinatorial approach, Advanced Energy Materials **7**, 1700866 (2017).

[15] N. Fleck, O. S. Hutter, L. J. Phillips, H. Shiel, T. D. C. Hobson, V. R. Dhanak, T. D. Veal, F. Jäckel, K. Durose, and J. D. Major, How oxygen exposure improves the back contact and performance of antimony selenide solar cells, ACS Applied Materials & Interfaces **12**, 52595 (2020).

[16] A. M. Huerta-Flores, L. M. Torres-Martínez, E. Moctezuma, and J. E. Carrera-Crespo, Novel $SrZrO_3$-Sb_2O_3 heterostructure with enhanced photocatalytic activity: Band engineering and charge transference mechanism, Journal of Photochemistry and Photobiology A: Chemistry **356**, 166 (2018).

[17] X. Li, X. Wang, X. Ning, J. Lei, J. Shao, W. Wang, Y. Huang, and B. Hou, Sb_2S_3/Sb_2O_3 modified TiO_2 photoanode for photocathodic protection of 304 stainless steel under visible light, Applied Surface Science **462**, 155 (2018).

[18] S. Kraut, E. A. Grant, J. R. Waldrop, and S. P. Kowalczyk, Precise determination of the valence band edge in x-ray photoemission spectra: application to measurement of semiconductor interface potentials, Physical Review Letters **44**, 1620 (1980).

[19] T. D. C. Hobson, L. J. Phillips, O. S. Hutter, H. Shiel, J. E. N. Swallow, C. N. Savory, P. K. Nayak, S. Mariotti, B. Das, L. Bowen, L. A. H. Jones, T. J. Featherstone, M. J. Smiles, M. A. Farnworth, G. Zoppi, P. K. Thakur, T.-L. Lee, H. J. Snaith, C. Leighton, D. O. Scanlon, V. R. Dhanak, K. Durose, T. D. Veal, and J. D. Major, Isotype heterojunction solar cells using n-type Sb_2Se_3 thin films, Chemistry of Materials **32**, 2621 (2020).

[20] N. Fleck, T. D. C. Hobson, C. N. Savory, J. Buckeridge, T. D. Veal, M. R. Correia, D. O. Scanlon, K. Durose, and F. Jäckel, Identifying Raman modes of Sb_2Se_3 and their symmetries using angle-resolved polarised Raman spectra, J. Mater. Chem. A **8**, 8337 (2020).

[21] T. D. C. Hobson, O. S. Hutter, M. Birkett, T. D. Veal, and K. Durose, Growth and characterization of Sb_2Se_3 single crystals for fundamental studies, 2018 IEEE 7th World Conference on Photovoltaic Energy Conversion (WCPEC) (A Joint Conference of 45th IEEE PVSC, 28th PVSEC & 34th EU PVSEC) , 0818 (2018).

[22] T. D. C. Hobson, L. J. Phillips, O. S. Hutter, K. Durose, and J. D. Major, Defect properties of Sb_2Se_3 thin film solar cells and bulk crystals, Applied Physics Letters **116**, 261101 (2020).

[23] H. Shiel, O. S. Hutter, L. J. Phillips, J. E. N. Swallow, L. A. H. Jones, T. J. Featherstone, M. J. Smiles, P. K. Thakur, T.-L. Lee, V. R. Dhanak, J. D. Major, and T. D. Veal, Natural band alignments and band offsets of Sb_2Se_3 solar cells, ACS Applied Energy Materials **3**, 11617 (2020).

[24] R. E. Williams, Q. M. Ramasse, K. P. McKenna, L. J. Phillips, P. J. Yates, O. S. Hutter, K. Durose, J. D. Major, and B. G. Mendis, Evidence for self-healing benign grain boundaries and a highly defective Sb_2Se_3-CdS interfacial layer in Sb_2Se_3 thin-film photovoltaics, ACS Applied Materials & Interfaces **12**, 21730 (2020).

[25] T. Hobson and K. Durose, Protocols for the miller indexing of Sb_2Se_3 and a non-x-ray method of orienting its single crystals, Materials Science in Semiconductor Processing **127**, 105691 (2021).

[26] D. A. Shirley, High-resolution x-ray photoemission spectrum of the valence bands of gold, Phys. Rev. B **5**, 4709 (1972).

[27] A. Proctor and P. M. A. Sherwood, Data analysis techniques in x-ray photoelectron spectroscopy, Analytical Chemistry **54**, 13 (1982).

[28] B. A. D. Williamson, T. J. Featherstone, S. S. Sathasivam, J. E. N. Swallow, H. Shiel, L. A. H. Jones, M. J. Smiles, A. Regoutz, T.-L. Lee, X. Xia, C. Blackman, P. K. Thakur, C. J. Carmalt, I. P. Parkin, T. D. Veal, and D. O. Scanlon, Resonant Ta doping for enhanced mobility in transparent conducting SnO_2, Chemistry of Materials **32**, 1964 (2020).

[29] J. E. N. Swallow, B. A. D. Williamson, S. Sathasivam, M. Birkett, T. J. Featherstone, P. A. E. Murgatroyd, H. J. Edwards, Z. W. Lebens-Higgins, D. A. Duncan, M. Farnworth, P. Warren, N. Peng, T.-L. Lee, L. F. J. Piper, A. Regoutz, C. J. Carmalt, I. P. Parkin, V. R. Dhanak, D. O. Scanlon, and T. D. Veal, Resonant doping for high mobility transparent conductors: the case of mo-doped In_2O_3, Mater. Horiz. **7**, 236 (2020).

[30] N. Tigau, V. Ciupina, and G. Prodan, The effect of substrate temperature on the optical properties of polycrystalline Sb_2O_3 thin films, Journal of Crystal Growth **277**, 529 (2005).

[31] C. Wood, B. van Pelt, and A. Dwight, The optical properties of amorphous and crystalline Sb_2O_3, physica status solidi (b) **54**, 701 (1972).

[32] B. Wolffing and Z. Hurych, Photoconductivity in crystalline and amorphous Sb_2O_3, physica status solidi (a) **16**, K161 (1973).

[33] J. E. N. Swallow, C. N. Savory, P. A. E. Murgatroyd, L. A. H. Jones, M. Smiles, T. J. Featherstone, H. Shiel, N. Fleck, T. D. C. Hobson, V. R. Dhanak, P. K. Thakur, T.-L. Lee, A. Regoutz, D. O. Scanlon, and T. D. Veal, Role of sb $5s^2$ lone pairs on the electronic structure of sb-chalcogenides (Sb_2O_3, Sb_2S_3, Sb_2Se_3 and Sb_2Te_3), Unpublished.

[34] O. S. Hutter, L. J. Phillips, K. Durose, and J. Major, 6.6% efficient antimony selenide solar cells using grain structure control and an organic contact layer, Solar Energy Materials Solar Cells **188**, 177 (2018).

[35] J. B. Mann, T. L. Meek, and L. C. Allen, Configuration energies of the main group elements, Journal of the American Chemical Society **122**, 2780 (2000).

[36] A. Walsh, D. J. Payne, R. G. Egdell, and G. W. Watson, Stereochemistry of post-transition metal oxides: revision of the classical lone pair model, Chemical Society Reviews **40**, 4455 (2011).